Journal of Molecular Liquids 318 (2020) 114304

Contents lists available at ScienceDirect

Journal of Molecular Liquids

journal homepage: www.elsevier.com/locate/molliq

Various metal organic frameworks combined with imidazolium, quinolinum and benzothiazolium ionic liquids for removal of three antibiotics from water

Alula Yohannes [a], Jing Li [b,*], Shun Yao [a,*]

[a] School of Chemical Engineering, Sichuan University, Chengdu 610065, China
[b] School of Life Sciences, Sichuan University, Chengdu 610065, China

ARTICLE INFO

Article history:
Received 20 July 2020
Received in revised form 8 September 2020
Accepted 10 September 2020
Available online 16 September 2020

Keywords:
Ionic liquid
Metal organic framework
Adsorption
Chlorotetracycline
Oxytetracycline
Tetracycline

ABSTRACT

In this research, imidazolium, quinolinum and benzothiazolium based ionic liquids (ILs) were immobilized on a metal organic framework (MOF) by solvent impregnation or capillary action. The synthesized IL@MOF composite materials were characterized by FTIR, XRD, SEM and TGA methods and then applied in removal of tetracyclines (TCs) from aqueous samples. The presence of ionic liquids significantly improved the adsorption efficiency of the metal organic framework, with 82% or higher removal percentage was obtained for the three target TCs while the pristine MOFs adsorption efficiency was below 50%. This could be attributed to the ability of ILs to make complex interaction with target drugs via multiple intermolecular forces. Experimental results revealed the effects of three significant factors including pH, temperature and solid-liquid ratio, and optimum adsorption efficiency could be achieved at pH 8 and 30 °C when solid-liquid ratio = 1:2 was adopted. The adsorption kinetics was properly fitted with pseudo-second order model and Redlich-Peterson model could be used to describe the adsorption isotherm for three antibiotics; moreover, the adsorption was an endothermic and spontaneous process in nature. Finally, the adsorbed TCs could be desorbed efficiently and the performance of the IL@MOF sorbent was further verified by actual water samples.

1. Introduction

Currently, more and more chemical substances are being released to the environment with the rapid development of medical care and pharmaceutical industry together with drug abuse. Many residual drugs have been found in various water resources [1,2]. Tetracyclines (TCs) are the prototypical broad-spectrum antibiotics and are occasionally used as first-line agents for the treatment of mild acute exacerbations of chronic bronchitis [3,4]. However, the widespread use of tetracyclines has resulted in a steady increase in the prevalence of resistance to these agents; meanwhile more and more TCs are detected in environment for their overuse in human health care together with livestock, agriculture, aquaculture, and bee-keeping [5–7]. Among the main TCs, tetracycline (TC), oxytetracycline (OTC) and chlorotetracycline (CTC) are three famous members which are very effective against gram-positive/negative aerobic and anaerobic bacteria. They have been found to be common pollutants in rivers, lakes, ground water and drinking water. In China, the traditional process of water treatment plants can not completely remove these trace antibiotics (the residual concentration is usually one billionth or even one trillionth) [8]. Moreover, the daily monitoring and analysis for water resources also need powerful and effective pre-treatment and enrichment means. Overall, adsorption is a common technique in both the removal and detection for related pollutants in nature.

Owing to tailorable porous structures and numerous active sites, metal organic frameworks (MOFs) have attracted considerable attention for adsorption technology, which are known as kind of unique hybrid crystalline materials constructed via self-assembly mechanism between metal ions or nodes and organic molecules [9,10]. By virtue of larger surface area and superior adsorption effect, they have more effective and efficient removal capacity of contaminants from water compared to other traditional porous materials. Hence, related studies have become a hot topic in the fields of chemistry, materials and environment [11–14]. Meanwhile, as green designer solvents, ionic liquids (ILs) have been proved with strong separation capacity for various kinds of organic compounds in current reports, which are expected to show great potential in above fields after flexible immobilization on different supports [15–20].

Despite there is great potential of IL@MOF composites in separation science, limited studies have been conducted for their use in liquid phase adsorption of TCs. Jhung and co-workers [21] incorporated 1-butyl-3-methylimidazolium chloride into the pores of MIL-101 by means of simple impregnation for removal of benzothiophene from

* Corresponding authors.
E-mail addresses: ljtjf@126.com (J. Li), cusack@scu.edu.cn (S. Yao).

https://doi.org/10.1016/j.molliq.2020.114304
0167-7322/

liquid fuel. Later on, the same research group synthesized the IL inside MIL-101 porous cavities via a ship-in-bottle (SIB) technique for similar objectives [22]. In this work, it aimed to explore several ILs and MOFs when combined produces synergetic effect for successful adsorptive elimination of TCs from water samples. To the best of our knowledge, no other published work attempted to investigate IL@MOF in the same application for the three representative TCs.

2. Experimental

2.1. Materials and instruments

Ethanol, zinc nitrate hexahydrate ($Zn(NO_3)_2 \cdot 6H_2O$, 99%), 2-methylimidazole (99%), benzene-1,3,5-tricarboxylic acid (H3BTC, 95%), terephthalic acid (98%), chromium chloride ($CrCl_3 \cdot 6H_2O$, 96%), copper nitrate hemipentahydrate $Cu(NO_3)_2 \cdot 5H_2O$, fluoroboric acid, 8-hydroxyquinoline, phosphoric acid, chlorotetracycline, oxytetracycline and tetracycline were supplied by Kelong Chemicals (Chengdu, China). Benzothiazole, methyl bromide and sodium hexafluorophosphate were supplied by Sigma-Aldrich Co. Ltd. (USA). Ultrapure water was attained by a water purification system A10 MilliPore (Bedford, MA). The ten ionic liquids with three main types of cations and four kinds of anions were chosen for this study, including 1-butyl-3-methylimidazolium chloride ([C_6MIM][Cl], **1**), 1-hexyl-3-methylimidazolium chloride ([C_4MIM][Cl], **2**), 1-butyl-3-methylimidazolium tetrafluoroborate ([C_4MIM][BF_4], **3**), 1-hexyl-3-methylimidazolium tetrafluoroborate ([C_6MIM][BF_4], **4**), 1-butyl-3-methylimidazolium hexafluorophosphate ([C_4MIM][PF_6], **5**), 1-hexyl-3-methylimidazolium hexafluorophosphate ([C_6MIM][PF_6], **6**), benzothiazolium tetrafluoroborate ([HBth][BF_4], **7**), benzothiazolium hexafluorophosphate ([HBth][PF_6], **8**), 8-hydroxyquinolinephosphate ([HOQu][H_2PO_4], **9**), and 8-hydroxyquinolinesulfate ([HOQu][HSO_4], **10**) were synthesized in our lab, which were identified by their melting points and spectral absorbance. All the structures of TCs and ILs are shown in Scheme 1.

Infrared Spectroscopy L1600300 (PerkinElmer, Fremont, USA) was utilized for identification of function groups of the composite IL@ZIF material. The size and image of microcrystals was viewed with JSM-7001F scanning electron microscopy (SEM) (JEOL Co., Ltd., Tokyo, Japan) and X-ray diffraction (XRD) patterns were recorded on a D8 type X-ray diffractometer fitted with accessional analytical system (Bruke, Karlsruhe, Deutschland). Thermogravimetric analysis (TGA) was implemented using TG 209 Fl Iris instrument (NETZSCH-Gerätebau GmbH, Selb, Deutschland) with heating rate of 10 °C min^{-1} from 30 to 800 °C under nitrogen. For evaluation of adsorbed target TCs UV–Vis spectrometer TU-1810 (Purkinje General Instrument Co., Ltd., Beijing, China) was used.

2.2. Preparation of candidate ionic liquids

Firstly, the synthesis of quinolinum ionic liquids was made following the procedures previously reported by our group with minor modifications [23]. Typically, 8-hydroxyquinoline (0.05 mol) was dissolved in 50 mL anhydrous ethanol under stirring at 5 °C in an ice bath. Then, phosphoric acid (0.05 mol) dissolved in 30 mL anhydrous ethanol was added dropwise into the aforementioned solution over a period of 30 min. After 4 h, the residual ethanol was removed under vacuum and the crude products were washed three times with 15 mL acetone. The obtained crude product was recrystallized from anhydrous ethanol and further purified by recrystallization from mixed solution of ethyl acetate and ethanol. At last, the crystals were filtered and pale pink needle-like crystals were obtained. [HOQu][HSO_4] was prepared under the same procedure except that different acid (sulfuric acid) was used. As a result, the yield of [HOQu][HSO_4] was 97%.

Secondly, the synthesis of benzothiazole tetrafluoroborate ([HBth][BF_4]) and hexafluorophosphate ([HBth][PF_6]) was carried out by referring the procedure previously developed in our lab via "one-pot" method [24]. The typical procedure is as follows. (1) 0.05 mol (6.7590 g) benzothiazole, 0.06 mol methyl bromide and 0.06 mol sodium hexafluorophosphate or 0.06 mol fluoroboric acid were placed in a 50 mL round-bottom flask equipped with a magnetic stirrer; (2) The reaction mixture was reacted for 6 h at 100 °C, and yellow paste crude product was collected. It was mixed with proper amount of distilled water and filtered to remove unreacted salts. The filter cake was washed with 10 mL ether for three times, and then washed with distilled water until there was no precipitate formation in the washed water with the silver nitrate test. The filter cake was recrystallized from hot anhydrous ethanol and colorless flake crystal was finally obtained after vacuum dryness. The yields of these benzothiazolium ILs were in the range of 92%–97%.

Finally, the following imidazolium ILs were synthesized according to previously reported procedures [25]:1-butyl-3-methylimidazolium chloride ([C_6MIM][Cl]), 1-hexyl-3-methylimidazolium chloride ([C_4MIM][Cl]), 1-butyl-3-methylimidazolium tetrafluoroborate ([C_4MIM][BF_4]), 1-hexyl-3-methylimidazolium tetrafluoroborate ([C_6MIM][BF_4]), 1-butyl-3-methylimidazolium hexafluorophosphate ([C_4MIM][PF_6]), 1-hexyl-3-methylimidazolium hexafluorophosphate ([C_6MIM][PF_6]). The reaction process was described briefly as follows: bromobutane (0.8 mol) and *N*-methylimidazole (0.1 mmol) were mixed in a round bottom flask at 82 °C under refluxing and stirring. After stirring for 24 h, the residual solvents were removed under vacuum at 40 °C. Then the resulting [[C_4MIM]Br products were washed with appropriate solvents and were placed in a vacuum drying oven for 24 h. Proportional mole ratio of [[C_4MIM]Br and $NaBF_4$ were made to react using acetone as solvent for 10 h at 40 °C under vigorous agitation. The reaction product was separated, and dichloromethane was added to the residue of reaction mixture, and white solids precipitate was recovered. In the next step, the solid product was isolated by filtration while the IL ([C_4MIM][BF_4]), was vacuum dried in an oven at 80 °C for 2 h to avoid the residual dichloromethane. In a similar fashion, ([C_4MIM][Cl]) and ([C_4MIM][PF_6]) were prepared by using HCl and KPF_6 instead of $NaBF_4$. Moreover, ([C_6MIM][Cl]), ([C_6MIM][BF_4]) and ([C_6MIM][PF_6]) were prepared by using bromohexane instead of bromobutane. The yields of these imidazolium ILs were in the range of 90%–94%.

2.3. Synthesis of IL@MOF (ZIF-8)

The standard method of MOF synthesis is solvothermal method in which reactants are mixed in high boiling polar solvents such as water, dialkyl formamides, dimethyl sulfoxide or acetonitrile [26]. Hydrothermal method is a subset of solvothermal method which uses water as a solvent. In the following part, three kinds of MOF materials (including ZIF-8, MIL-101 and HKUST-1) were firstly synthesized in previous ways [27–29] and then combined with the former ILs.

The former reported strategy for the synthesis of IL@MOF composites was based on ionothermal method by the use of an IL as both the solvent and template or structure-directing agent [30]. However, cations are not able to show similar physicochemical behaviors as the bulk ILs, which is a disadvantage for subsequent applications. The recent strategy towards the synthesis of IL@MOF composite involves heterogenization of ILs based on post-synthetic modification of MOFs. The typical procedure for the synthesis of IL@ZIF-8 by wet impregnation was as follows: certain amount of the previously synthesized IL was weighed and placed in an Erlenmeyer flask. Then 3 mL of methanol was added to the flask containing IL, and the vial was gently mixed until the IL was dissolved. The total amount of ionic liquid used for the impregnation varied depending on the maximum value of IL desired in the resulting composite. The solution was added dropwise to the preweighted ZIF-8 material, and the composite was dried at 70 °C overnight to remove any remaining solvent and stored in a desiccator. In another strategy called capillary action, the IL and MOF are directly mixed without using a solvent and ILs are loaded into the pores of MOFs through capillary action. The MOF is first dried to remove all impurities from the pores before being mixed with the IL.

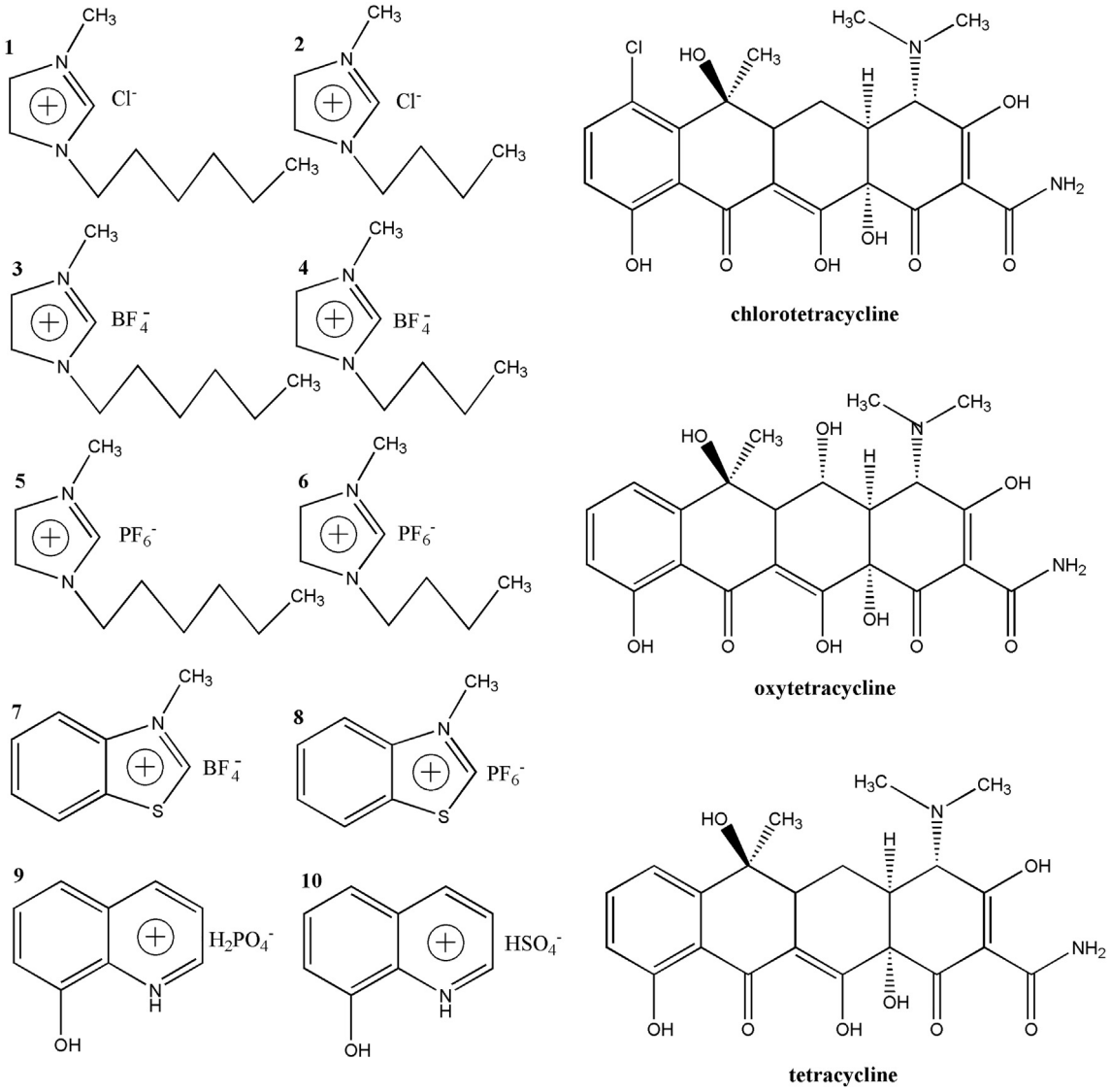

Scheme 1.

Then, the two materials are mixed by using a mortar and a pestle at a certain volumetric occupancy ratio. To ensure better diffusion of the IL into the pores of the MOF, the resulting sample is heated overnight and then the resulting powder was stored in a closed desiccator.

2.4. Adsorption experiments

Certain dosage of the synthesized IL@MOF, after being heated at 150 °C, was mixed with 20 mL sample solution containing target TCs with desired concentration in 50 mL Erlenmeyer flask. Then, the flasks were sealed and placed in a water-bath oscillator for agitation with shaking speed of 100 rpm for certain duration of time as well as temperature. After completion of adsorption step, the flasks were subjected to centrifugation at 6000 rpm for 5 min and the adsorbent settled at the bottom of the centrifuge tube was decanted from the supernatant. At last, the amount of adsorbate left in the supernatant was determined by UV–visible spectrophotometer at 355 nm. Adsorption efficiency (E, %) was calculated based on determined concentrations of chlorotetracycline; oxytetracycline and tetracycline before and after adsorption, respectively. The adsorption amount was calculated according to the following equations.

$$E(\%) = \frac{(C_0 - C_1) \times V}{(C_0 \times V)} \times 100\% = \frac{(C_0 - C_1)}{C_0} \times 100\% \quad (1)$$

$$q_e = \frac{(C_0 - C_1) \times V}{m} \quad (2)$$

where C_0 is the initial concentration and C_1 is the equilibrium concentration of TCs in the solution, respectively, V is the volume of the solution, and m is the mass of the adsorbent.

3. Results and discussion

3.1. Properties of IL@MOF adsorbents

In order to characterize the synthesized materials, FT-IR, XRD, SEM, and TGA methods were employed. Here [HBth][PF_6]@ZIF-8 is taken as an example and its FT-IR spectra is shown in Fig. 1a under the comparison with that of ZIF-8, which were recorded in the range of 4000–400 cm^{-1} in the transmission mode using Infrared L1600300 Spectroscopy with KBr pellets. The figure provides good evidence for successful incorporation of ILs into ZIF-8 from the changes in the peak

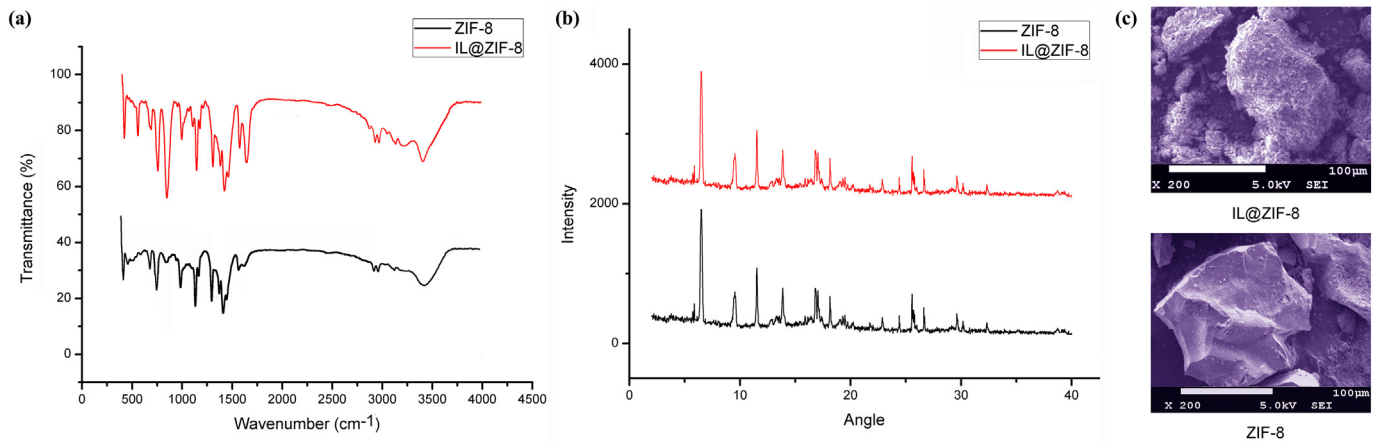

Fig. 1. (a) FTIR spectra (b) XRD pattern (c) SEM image of ZIF-8 and [HBth][PF_6]@ZIF-8.

intensities and appearance of additional peaks for IL@ZIF-8 associated with the bulk IL. The new peaks at 557 cm^{-1} (P—F bending) and 848 cm^{-1} (P—F stretching) prove the existence of PF_6^-. C—H bending vibrations and C—H rocking vibrations of benzene ring can be found below 1000 cm^{-1}, and the appeared peak at 1644 cm^{-1} for IL@ZIF-8 belongs to the strengthened C═N stretching vibrations. Similarly, the bands between 1100 cm^{-1} and 1000 cm^{-1} corresponds to asymmetric and in-plane bending vibration. Moreover, the spectra in the high frequency region such as, 3430, 2929 and 2800 cm^{-1} are attributed to C—N stretching vibration, asymmetric C—H stretching vibration and symmetric stretching vibrations, respectively. The difference in peak width of the spectra before and after modification as well as the higher peak intensity for the composite indicates an increasing absorbance with the loading amount of the IL [31,32].

Furthermore, D8 X-ray diffractometer fitted with accessional analytical system were used to obtain X-ray diffraction patterns of each composite material. As depicted in Fig. 1b, the diffraction peaks of the [HBth][PF_6]@ZIF-8 resembles with the XRD pattern of ZIF-8 indicating that crystallinity of the composite material remained intact. The XRD experiment illustrated that the crystal phases of pristine and modified MOFs have remarkable similarity, which is confirming successful synthesis and stability of the MOFs even after decorated with ionic liquids. JSM-7001F scanning electron microscopy was used to view the size and image of microcrystals. The SEM images presented in Fig. 1c show that the surface morphology of ZIF-8 changed after incorporation of ILs which indicates the existence of guests inside the pores of MOFs. As measured by N_2 adsorption experiments, the pore size of ZIF-8 was found within 0.98–2.79 nm, which also indicates it can accommodate all the tested IL molecules with the molecular diameter in the range of 10.0–13.0 Å.

Thermogravimetric analysis was done using TG 209 Fl Iris instrument with heating rate of 10 °C min^{-1} from 30 °C to 800 °C under nitrogen which helps to provide information of the chemical and mechanical stability. The measurement result revealed the synthesized composite adsorbent is stable up to nearly 200 °C as indicated in Fig. 2a and b. It could be observed that [HBth][PF_6]@ZIF-8 exhibited more weight loss than ZIF-8 which is associated with the loss of the corresponding components within the structure of bulk IL during high temperature thermal treatment. Particularly, when the temperature goes higher than 250 °C, 30% mass of the IL@ZIF-8 eliminated and further increase in temperature up to 450 °C results in total collapse of the composite material. For pristine ZIF-8, the first weight loss appeared around 350 °C and about 12% mass has been lost.

3.2. Separation conditions for adsorption

Current studies have proven MOFs to be an ideal adsorbent, and one way to upgrade the adsorption properties of them was to decorate them with ILs using a post-synthetic modification based on solvent impregnation. It is expected to bring a higher performance for adsorption than the pristine MOFs. Obviously, the different complex formation between target drug molecules and coordinatively unsaturated sites in three kinds of MOFs, and the number of open metal site play a crucial role in adsorption. Here ten different ionic liquids synthesized in our lab were tested as potential guests that are introduced into the pores of virgin MOFs targeted for the purpose of TCs adsorption. Tetracyclines are complex hydrophilic drugs having high solubility in water and can exist both in acidic and basic form. An initial amount of 10% ILs was impregnated together with MOFs for preliminary observation. Generally the ILs improves the adsorption efficiency of all the studied MOFs to a certain extent as can be seen from Fig. 3a for imidazolium type ILs and Fig. 3b for benzothiazolium and quinolinum ILs. The highest adsorption efficiency was obtained for the target TCs during the combination of [HBth][PF_6] with ZIF-8. It should be noted that except the HKUST-1 and IL@HKUST-1, the other MOFs and IL@MOF composites are stable in water. HKUST-1 is easy to absorb water, which can cause the collapse of the framework and the destruction of crystal structure. Therefore, HKUST-1 and IL@HKUST-1 based adsorption study was carried out in ethanol solution instead of aqueous solution. Besides the stability of the MOF support, the hydrophilicity of the ionic liquids could also contribute to the stability of the resulting composites. After careful investigation, hydrophobic [HBth][PF_6] was selected to be impregnated with ZIF-8 and the composite product was found very stable in aqueous media. After [HBth][PF_6]@ZIF-8 was mixed with water under stirring for 12 h (320 rpm), [HBth][PF_6] was not detected in the water sample with methanol as solubilizer by using ultraviolet spectroscopy at its λ_{max} of 278 nm. Besides that, the preparation conditions of ZIF-8 are much milder (1 h at ambient temperature) than the other two (8 h at 210 °C for MIL-101, and 24 h at 110 °C for HKUST-1, respectively).

Moreover, the best result for OTC was specifically obtained by the IL@MOF formed through wet impregnation when [HBth][PF_6] to ZIF-8 ratio was increased to 25% as depicted on Fig. 3c. The improved adsorption properties of the IL@MOFs could be due to the capability of ILs to create complex interactions (e.g. H-bond and π-π stacking) with TCs. When the percentage is beyond 25%, the IL will be overloaded and a part of it will gather unsteadily on the MOF surface and then fall off during adsorption, so E (%) begins to decline. As ideal sorbent, [HBth][PF_6] was mixed with ZIF-8 according to the preset percentage of 25% for the following experiment, and the actual IL content was verified to be 23.3 ± 0.2% (average 0.789 mmol/g) on the basis of calculation with the sulfur content (S atom in benzothiazole cation) in the final composite of IL@MOF, which was determined by EA 3000 element analyzer (Euro Vector, Italy). For comparison with above wet impregnation, the loading way of IL with capillary action was carried out in another

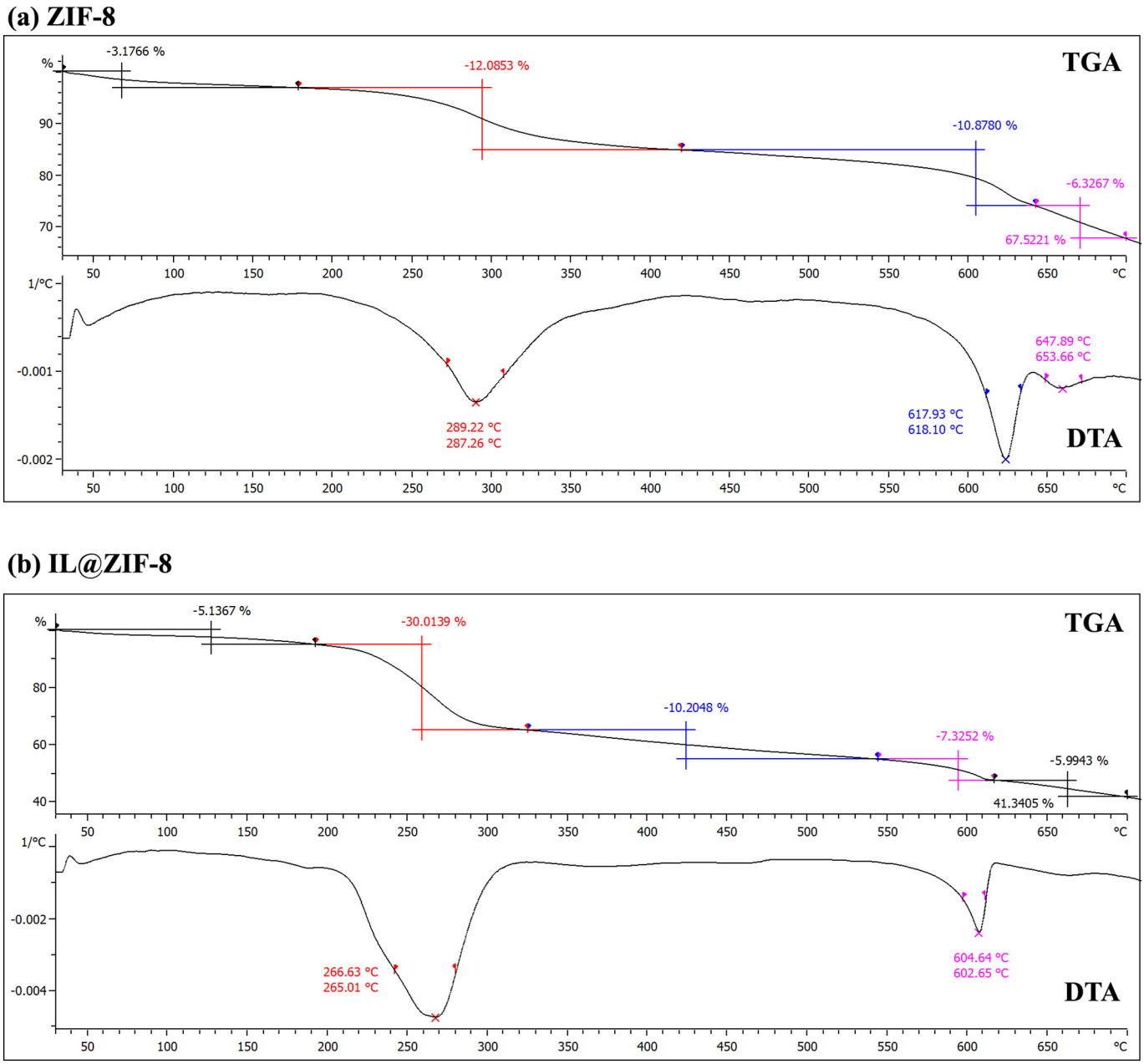

Fig. 2. Thermogravimetric analysis of (a) ZIF-8 and (b) [HBTh][PF_6]@ZIF-8.

investigation and the [HBth][PF_6] was mixed with activated ZIF-8 powders using mortar and pestle in a molar ratio of 0.20:1, 0.25:1, 0.30:1 and 0.35:1. The mixture was heated and stored overnight to enhance the diffusion of the IL through pores of ZIF-8. As shown in Fig. 3d, the adsorbed quantities of TCs increased to a significant extent until the IL to MOF ratio became 0.30 to 1. The capillary action improves the confinement of IL inside ZIF-8 pores and hence, the stability of the resulting composite, which brought great potential in the way of increasing the adsorption efficiency of TCs.

Fig. 4a shows the adsorption progress with time while other condition kept as follows: 10 mg L^{-1} oxytetracycline (OTC), 5 mg IL@ZIF-8, 20 mL sample solution, neutral pH and room temperature. The adsorption results showed that the amount of OTC adsorbed with time almost reached a plateau in 1 h. Fig. 4b demonstrates the effect of initial concentration on the adsorption behavior of TCs in static adsorption mode for 1 h at room temperature. When the sample concentration exceeds higher than 40 mg L^{-1}, adsorption progress remain constant, indicating that the active sites of adsorbent are fully saturated and no further retention of TCs occurs. Fig. 4c shows the effect of solid-liquid ratio in the adsorptive removal of TCs from aqueous solution. The adsorption capacity was calculated for the removal of OTC with 40 mg L^{-1} concentration and 20 mL sample solution volume. The adsorption amount increased with the increment of IL@ZIF-8 until solid-liquid ratio of 10:20 (mg:mL^{-1}). Fig. 4d provides the trend in adsorption performance with the increment of temperature. The adsorbed amount of OTC increased at higher temperature, indicating that temperature plays an important role in this particular adsorption phenomenon. Fig. 4e depicts the influence of pH on the adsorption of TCs from aqueous solutions. The pH level determines the physicochemical properties of target drugs particularly, their acidity and electrostatic interaction behaviors. The maximum adsorption capacity of the composite IL@ZIF-8 adsorbent for target OTC was observed when pH was set at 8.

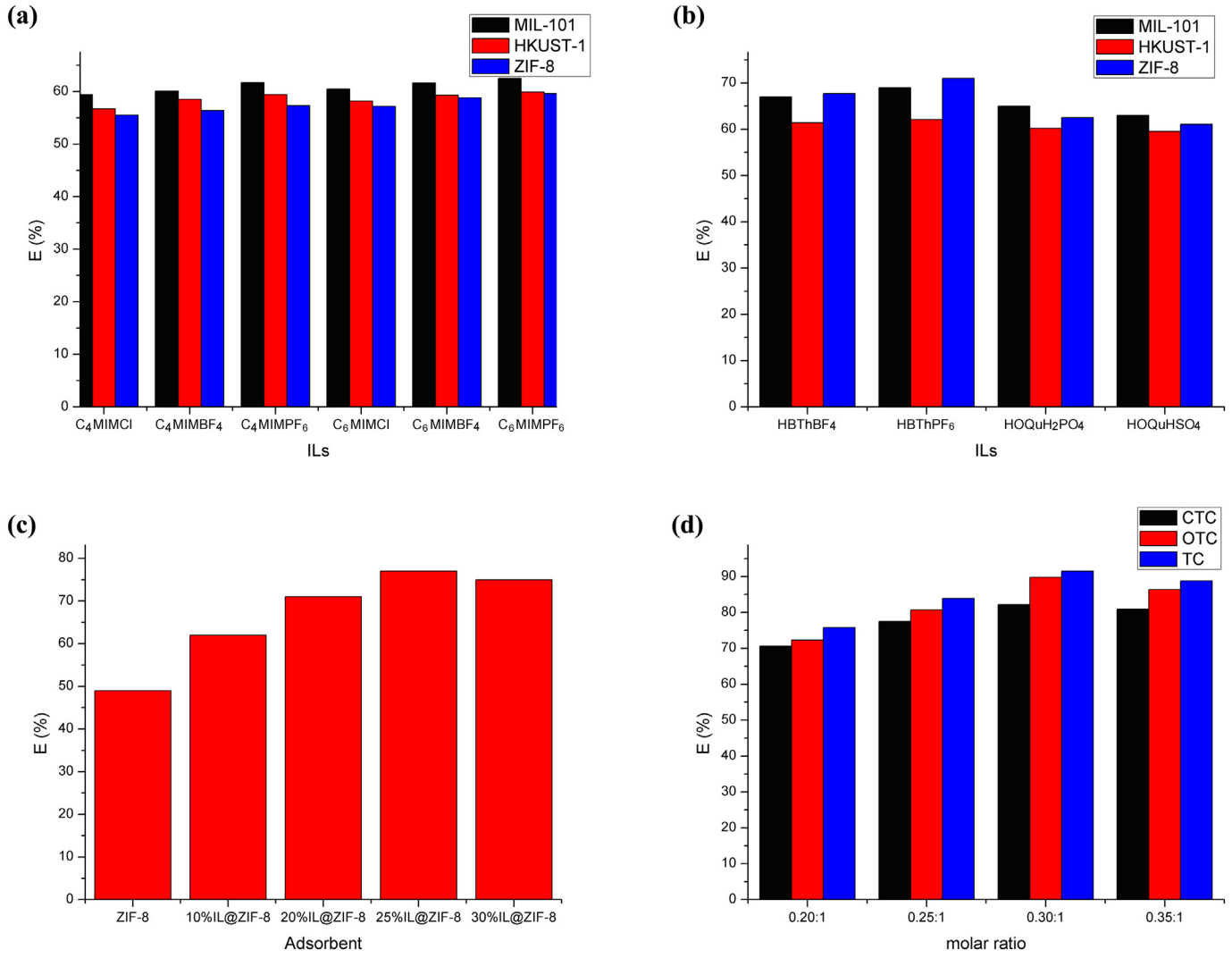

Fig. 3. Effects of (a) benzothiazolium ILs, (b) imidazolium ILs, (c) IL percentage and (d) molar ratio on extraction efficiency.

Three selected factors including effects of pH, temperature and solid-liquid ratio on the adsorptive removal efficiency of OTC were further optimized using response surface methodology and Box-Behnken experimental (BBE) design. For the three variables, Box-Behnken design requires a total of 17 experiments in order to determine the optimum response as given in Table 1.The variables were examined at three levels set as follows: pH (7, 8 and 9), Temperature (25, 30 and 35 °C) and solid-liquid ratio (5:20, 10:20, and 15:20).The response model coefficients were estimated by Design Expert 7.0.0 software. The 3D response surface and contour plot for the effects of temperature vs. pH, solid-liquid ratio vs. pH and solid-liquid ratio vs. temperature are depicted in Fig. 4f, g and h. The second order polynomial response model obtained from the experimental design is given in Table 1. The R^2 value is 0.9973 which proved that model is appropriate to predict the optimum values. The "Pred R-Squared" of 0.9579 is in reasonable agreement with the "Adj R-Squared" of 0.9939.The Model F-value of 288.60 implies the model is significant. There is only a 0.01% chance that a "Model F-Value" this large could occur due to noise. The "Lack of Fit F-value" of 57.07 implies the Lack of Fit is significant. There is only a 0.10% chance that a "Lack of Fit F-value" this large could occur due to noise. It could be deduced that the optimum levels of all three variables are as follows: pH = 8, temperature = 30 °C and solid-liquid ratio = 10:20.

3.3. Adsorption kinetics

Investigation of adsorption kinetics helps to verify the rate of removal of TCs and provide some relevant data for subsequent study of adsorption mechanism. The experimental data were obtained in a batch process after conducting adsorption at three different initial concentrations and varying contact time in order to check the time period where the adsorption process was completed. For identification of rate limiting steps and determination of available adsorption sites at a given time kinetic modelling is used in the design of appropriate adsorption technology. The commonly used kinetic models including pseudo-first-order, pseudo-second-order and Weber–Morris model were considered to fit with the experimental data. The kinetic study was carried out from 10 min to 60 min at two different initial concentrations (20 and 40 mg L^{-1}) under optimized conditions.

Fig. 4. Investigation of adsorption conditions: (a) time, (b) TCs concentration, (c) solid to liquid ratio, (d) temperature, (e) pH and response surface between (f) temperature and pH, (g) S/L ratio and pH, (h) S/L ratio and temperature.

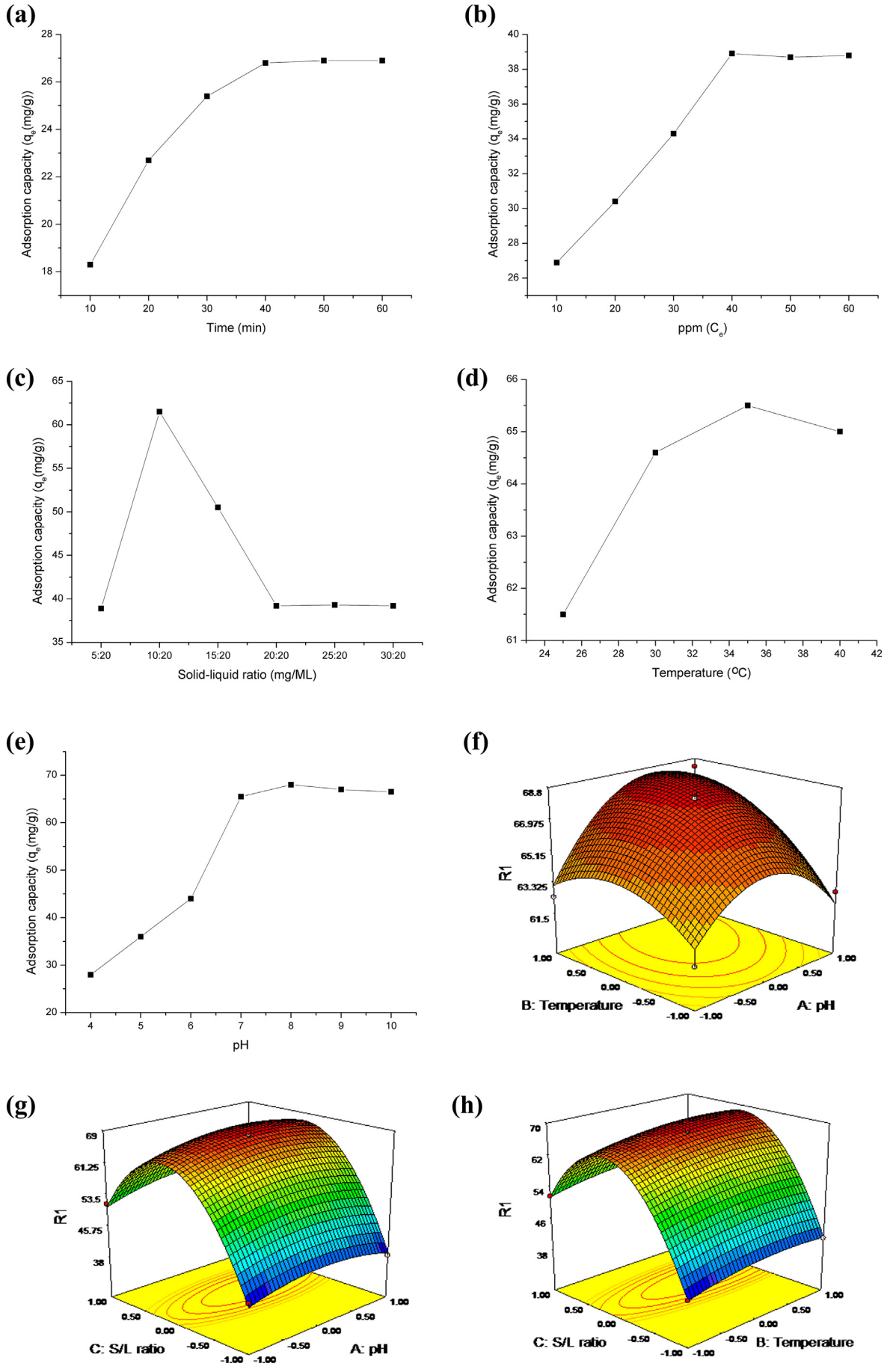
(a)
Adsorption capacity (q_e(mg/g))
Time (min)
(b)
Adsorption capacity (q_e(mg/g))
ppm (C_e)
(c)
Adsorption capacity (q_e(mg/g))
Solid-liquid ratio (mg/ML)
5:20
10:20
15:20
20:20
25:20
30:20
(d)
Adsorption capacity (q_e(mg/g))
Temperature (°C)
(e)
Adsorption capacity (q_e(mg/g))
pH
(f)
R1
68.8
66.975
65.15
63.325
61.5
B: Temperature
A: pH
(g)
R1
69
61.25
53.5
45.75
38
C: S/L ratio
A: pH
(h)
R1
70
62
54
46
38
C: S/L ratio
B: Temperature

Table 1
Box-Behnken design for 17 set of experiments.

Run	Variables			Response
	x_1 (pH)	x_2 (temperature)	x_3 (S/L ratio)	OTC
1	0 (8)	0 (30)	0 (10:20)	68.2
2	1 (9)	0 (30)	1 (15:20)	53.0
3	1 (9)	1 (35)	0 (10:20)	68.3
4	0 (8)	0 (30)	0 (10:20)	68.3
5	−1 (7)	−1 (25)	0 (10:20)	61.5
6	0 (8)	0 (30)	0 (10:20)	68.0
7	0 (8)	1 (35)	1 (15:20)	55.0
8	0 (8)	1 (35)	−1 (5:20)	41.2
9	0 (8)	0 (30)	0 (10:20)	68.5
10	0 (8)	−1 (25)	−1 (5:20)	38.7
11	−1 (7)	0 (30)	−1 (5:20)	39.6
12	1 (9)	0 (30)	−1 (5:20)	38.5
13	1 (9)	−1 (25)	0 (10:20)	62.8
14	−1 (7)	1 (35)	0 (10:20)	62.5
15	−1 (7)	0 (30)	1 (15:20)	51.4
16	0 (8)	0 (30)	0 (10:20)	68.3
17	0 (8)	−1 (25)	1 (15:20)	52.0

The pseudo-first-order (PFO) equation has been applied extensively to describe the sorption kinetics and in this case, the hypothesis is such that the rate of adsorption declines proportionally with the upsurge of adsorption capacity. The PFO model equation is expressed as follows:

$$\frac{dy}{dx} = k_1(q_e - q) \tag{3}$$

$$\log(q_e - q) = \log q_e - \frac{k_1}{2.303}t \tag{4}$$

where q_e is the adsorption capacity of the adsorbent at equilibrium and q is the adsorption capacity of the adsorbent at certain time, and k_1 is the rate constant which is a function of the adsorption environments computed from the graph of log ($q_e - q$) versus *t*. The graph comes to be a straight line and passing through the origin with a slope k_1 for those systems that comply with PSO model.

Pseudo-second-order (PSO) kinetic model hypothesis states that the kinetics of retaining target drugs is second order pertaining to the accessible adsorption sites and the rate-limiting step is the interplay among the existing adsorption sites and adsorbate. The PSO equation model is expressed as follows:

$$\frac{dy}{dx} = k_2(q_e - q)^2 \tag{5}$$

$$\frac{t}{q} = \frac{1}{k_2 q_e^2} + \frac{t}{q_e} \tag{6}$$

where k_2 is the PSO rate constant, qe is the adsorption capacity of the adsorbent at equilibrium and q the adsorption capacity of the adsorbent at certain time. The graph of t/q versus t appears as straight line for those adsorption systems go along with PSO model and slope obtained is used to determine the rate constant. The data fitted well with PSO model is attributed with chemisorption and the number of active sites on the sorbent determines the adsorption capacity.

Finally, Weber–Morris model assumes that the uptake of target drugs take place in two steps including intra-particle diffusion through the pores and the boundary layer diffusion on the surface. The intraparticle equation is given as following:

$$q_t = K_i t^{0.5} + C \tag{7}$$

where q_t is the retained amount of target molecule at time t, K_i is the intraparticle diffusion constant determined from the slope of q_t versus $t^{0.5}$ and C is the intercept for the width of boundary layer, the higher the intercept the bigger the boundary layer influence. As stated by Weber–Morris model, certainly intraparticle diffusion is the rate determining phase of the overall adsorption system if the graph of q_t versus $t^{0.5}$ yields a straight line passing through the origin.

As can be seen from Fig. 5a, the kinetic curves plot indicates the adsorption rate is faster in the first 40 min of contact time, then after the adsorption gradually increases before equilibrium is reached. The pseudo-second order model show the best fitting to the experimental data, as indicated by the high r^2 values provided in Table 2. It can be deduced that due to the presence of abundant adsorption sites the rate of adsorptive removal of tetracyclines increases rapidly in the initial stage and gradually decreases probably as a result of saturation of these free sites as they are taken by the adsorbates.

3.4. Adsorption isotherm

Adsorption isotherms can provide the relationship between the adsorption amount of TCs on the adsorbent and concentration of TCs remained in the sample solution when the adsorption equilibrium is reached. For this purpose, the experiments were conducted at three different temperatures with initial concentration of OTC ranging from 10 to 50 ppm as shown in Fig. 5b. Identifying the appropriate isotherm model plays a significant role in the design of suitable adsorption system which validates the adsorption process of the studied adsorbate-adsorbent system. In this regard, the maximum adsorption capacity of IL@ZIF-8 composite was evaluated by fitting the experimental data to three widely known adsorption isotherm models namely, Langmuir, Freundlich and Redlich-Peterson.

Langmuir model designates the type of explicit surface adsorption encompassing strong forces assuming that adsorption is carried out over a homogenous surface by monolayer adsorption devoid of any interplay among adsorbed molecules. In this case, there exists insufficient amount of adsorption sites and every single site hosts only one guest species, given by the following equation:

$$\frac{C_e}{q_e} = \frac{1}{Q_o b} + \frac{C_e}{Q_o} \tag{8}$$

where C_e is the concentration of target species at equilibrium, q_e describes the amount of target species retained at equilibrium, Q_o represents the maximum adsorption capacity of the composite material, and b represents a Langmuir constant related to the binding energy of adsorption. The data were fitted to the Langmuir model by plotting c_e/q_e against c_e, and the numerical figures of Q_o and b were computed from the slope and intercept of the curve.

Freundlich model is isotherm equation that can be accustomed to define a monolayer adsorption as well as a multilayer adsorption based on adsorption on a heterogeneous surface. Linear form of Freundlich isotherm equation can be expressed as following:

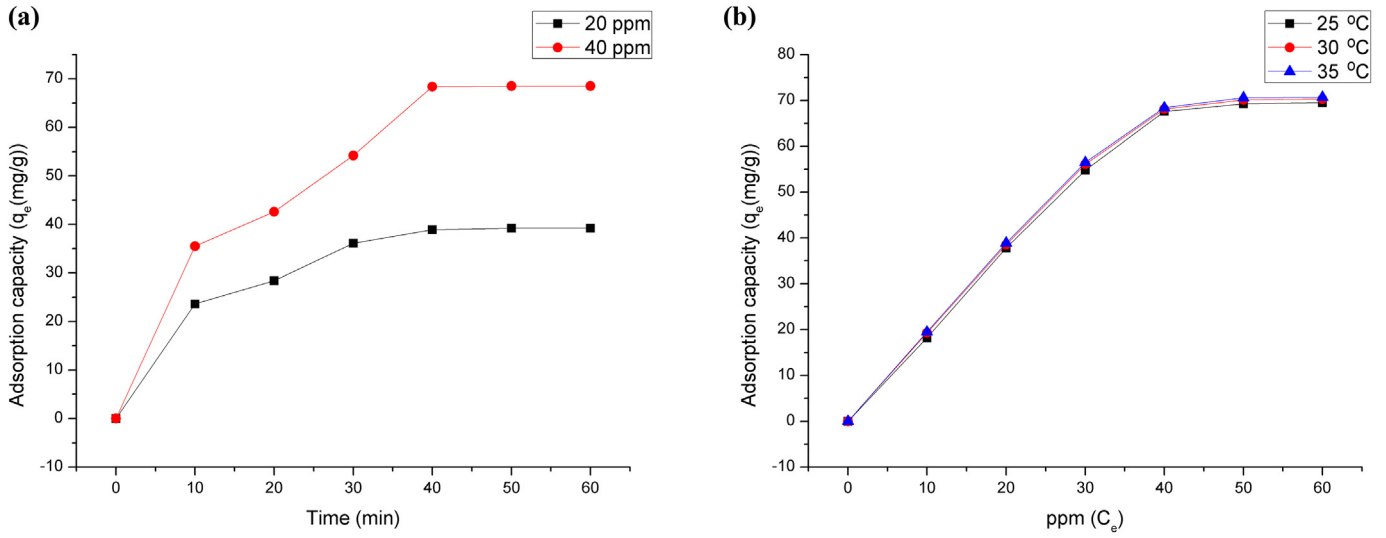

Fig. 5. (a) Adsorption kinetics and (b) adsorption isotherm.

$$Lnq_e = LnK_F + \frac{1}{n}LnC_e \quad (9)$$

where C_e is the concentration of target compounds at equilibrium, q_e is the amount target compounds retained at equilibrium, and K_F, n are numerical values related to retained species and sorbent material at a certain temperature.

Redlich-Peterson model is another alternative model that can be used to describe adsorption isotherm over a wide-ranging concentration level in both homogeneous and heterogeneous systems. It is a three parameter equation which brings both Langmuir and Freundlich isotherms together. However, only at low concentrations of adsorbate shows monolayer adsorption. The linear equation of the Redlich-Peterson model is given as following:

$$q_e = \frac{K_{RP}C_e}{1 + \alpha_{RP}C_e^{\frac{1}{n}}} \quad (10)$$

where K_{RP}, α_{RP} and $1/n$ are Redlich-Peterson constants and the exponent, $1/n$, lies between 0 and 1.

It is clear that with the increment of adsorption temperature the maximum adsorption capacity of the system increased to certain amount and reached to 70.7 mg g^{-1} at 25 °C. The adsorption isotherm parameters for the three models and the corresponding correlation coefficients, R^2, are calculated and the results are presented in Table 3. The higher determination coefficient close to unity, for Redlich-Peterson model is taken as a guarantee to use it as a model in order to estimate the equilibrium adsorption amount. The adsorptive removal process involves chemisorption and multilayer surfaces. The Langmuir adsorption is also suitable to estimate the equilibrium maximum adsorption capacity however; the determination coefficient is lesser than the Redlich-Peterson model. In this work the enhanced adsorption achievement is mainly ascribed to the presence of IL within the adsorbent which gets involved in various interactions. TCs have amphoteric property that led them potentially take part in acid-base interaction between their tertiary amine groups and the secondary building unit of ZIF-8 as well as with the cation of the IL, [HBth][PF_6]. Since the adsorption was carried in alkaline conditions, TCs became negatively charged ions. This observable fact favors the adsorption of TCs on the IL@ZIF-8 adsorbent. In addition, the aromatic group of TCs could come together with the aromatic rings of the IL in the IL@ZIF-8 through π-π stacking which ease the diffusion of TCs from the sample solution to the outer surface of adsorbent and subsequently into the pores and inner surface. For solid samples, IR is a useful tool to analyze the chemical circumstance of related groups and its minor change for interaction of adsorbate and adsorbent [33], and it was observed the peak intensity belonging to vibration of benzene ring skeleton (1450–1600 cm^{-1}) for IL@MOF became weaker, which indicated its vibration was restricted by π-π interaction with TCs. Moreover, the peaks at 557 cm^{-1} (P—F bending) and 848 cm^{-1} (P—F stretching) were shifted to 548 and 836 cm^{-1} by H-bonds between PF_6^- and hydroxyl/carbonyl groups of TCs. At the same time, their intensity was reduced, which indicated some anion-exchange occurred between PF_6^- and negatively charged TCs. Above findings accorded with the mechanism of chemisorption, which has been revealed by PSO model.

Table 2
Kinetic models and corresponding parameters calculated from experimental data.

Kinetic models	Parameters	Concentrations	
		20 ppm	40 ppm
Pseudo-first order	q_e (mg g^{-1})	39.2	68.5
	k_1 (min^{-1})	0.397	0.236
	R^2	0.922	0.934
Pseudo-second order	q_e (mg g^{-1})	39.2	68.5
	k_2 (g mg^{-1} min^{-1})	0.095	0.034
	R^2	0.998	0.999
Weber–Morris	C (mg g^{-1})	15.9	32.7
	K_i (mg g^{-1} $min^{-0.5}$)	1.244	1.035
	R^2	0.876	0.778

Table 3
Isotherm models and corresponding parameters calculated from experimental data.

Isotherm models	Parameters	Temperature		
		25 °C	30 °C	35 °C
Langmuir	Q_o (mg g^{-1})	69.5	70.3	70.7
	K_L (L mg^{-1})	0.158	0.166	0.174
	R^2	0.899	0.898	0.895
Freundlich	1/n	0.936	0.733	0.425
	K_F (mg^{1-n} L^n g^{-1})	9.544	12.454	15.667
	R^2	0.786	0.789	0.788
Redlich-Peterson	α (L mg^{-1})	14.5	12.7	10.9
	K (L mg^{-1})	1.987	2.143	2.466
	1/n	0.675	0.689	0.744
	R^2	0.998	0.999	0.999

Table 4
Thermodynamic parameters calculated from experimental data.

C_o (mg L^{-1})	ΔH (kJ mol^{-1})	ΔS (kJ mol^{-1} K)	ΔG (kJ mol^{-1})		
			25 °C	30 °C	35 °C
10	13.9	0.0652	−5.5296	−5.8556	−6.1816
20	11.6	0.0535	−4.3430	−4.8780	−4.8780
30	14.4	0.0586	−3.0628	−3.3558	−3.6488
40	14.1	0.0552	−2.3496	−2.6256	−2.9016
50	12.4	0.0485	−2.0530	−2.2955	−2.5380
60	11.8	0.0458	−1.8484	−2.0774	−2.3064

3.5. Adsorption thermodynamics

Adsorption thermodynamics give essential knowledge about the spontaneous nature of the whole system and guide to evaluate the influence of temperature on adsorption mechanism. A brief thermodynamics analysis was carried out using adsorption isotherm data at three different temperatures (25 °C, 30 °C and 35 °C). The thermodynamics results were given in Table 4. The calculation of basic thermodynamic parameters such as, entropy (ΔS), free energy (ΔG) and enthalpy (ΔH) was obtained by using the following equations:

$$\Delta G = -RT \ln K_c \tag{11}$$

$$\Delta G = \Delta H - T\Delta S \tag{12}$$

$$K_c = \frac{q_e}{C_e} \tag{13}$$

$$\ln K_c = \frac{\Delta S}{R} - \frac{\Delta H}{RT} \tag{14}$$

where q_e is the amount retained species per unit mass of sorbent material at equilibrium, C_e is the concentration of sorbent material at equilibrium, R is the universal gas constant, K_c is the value of equilibrium constant at standard temperature and pressure and T denote the solution absolute temperature. The numerical figures of enthalpy and entropy are computed from the graphical plot of $\ln K_c$ versus 1/T particularly, from the calculated values of slope and intercept of the curve.

For adsorption phenomena to be spontaneous process, energy at the end of the process must be less than the initial state. The values of ΔG became more negative when the temperature increased from 25 °C to 35 °C, proving the spontaneous adsorption of target antibiotics onto IL@ZIF-8 and improved adsorption at higher temperature. The positive value of ΔH indicates the endothermic nature of adsorption and the adsorption capacity enhanced with raising temperature. Moreover, the positive values of ΔS proved the randomness during adsorption which reflects the thermodynamically favorable nature of the overall system.

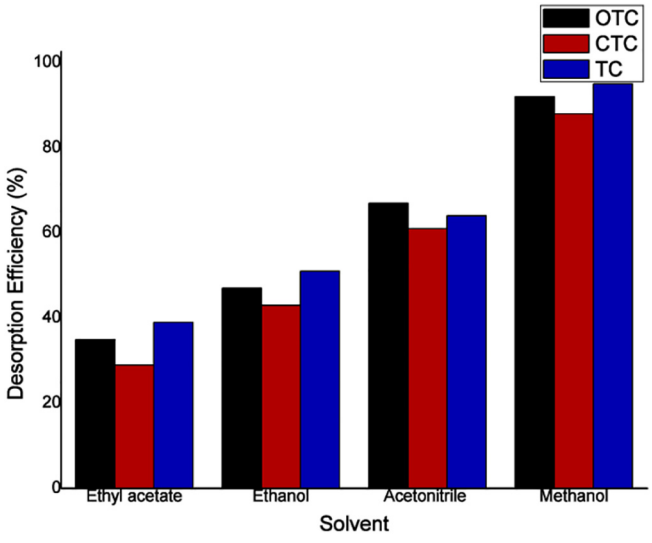

Fig. 6. Desorption efficiency for OTC, CTC and TC using various solvents.

3.6. Desorption and application for actual samples

The reusability of composite material is incredibly important criteria with the intention to evaluate the adsorption potential and feasibility in relation to the prestige for practical use. Promising adsorbents show very stable performance for several adsorption-desorption cycles that help to minimize the operational cost by recycling for use in several times. After absorption-desorption procedure these adsorbents are washed, dried and reused again and again. For this purpose, desorption experiments were carried out in batch mode using various solvents/eluents. As can be seen from Fig. 6, better desorption efficiency was obtained with methanol and desorption efficiency could be calculated as following:

$$D(\%) = \frac{C_2 \times V_2}{(C_0 - C_1)V_0} \times 100\% \tag{15}$$

where D is the desorption efficiency, C_0, C_1 and C_2 (mg L^{-1}) denote the concentration of TCs in the initial solution, the supernatant and desorption solution, respectively; V_0 represents the volume of initial solution and V_2 represents the volume of eluent. In summary, efficient desorption is beneficial and necessary for good reuse of the IL@MOF adsorbent.

Furthermore, the ground and surface actual water samples were collected from different sites near Lake Ziway (located within the Great Rift Valley of Ethiopia, 160 km away from the capital city Addis Ababa), and the area around the lake is well known by horticulture and dairy farming which are the possible sources of TCs within the collected water samples. All the samples were filtered with 0.45 μm membrane before the adsorption experiment, and then 20 mL sample was adsorbed by 10 mg [HBth][PF_6]@ZIF-8 at 30 °C and pH 8 for an hour. The adsorption result indicates TCs were not captured in the ground water samples; whereas 40.0 mg L^{-1} TCs were removed from the surface water samples. Therefore, it is highly recommended to apply novel adsorption technologies, like the one developed here, to effectively remove potential antibiotics and other chemically related drug substances from the aquatic environment.

4. Conclusions

Ten IL@MOF composites were synthesized using imidazolium, quinolinum and benzothiazolium type ionic liquids and ZIF-8 metal organic framework. The successful syntheses of the composites were confirmed after the study of their morphology, crystallinity, characteristic functional groups and thermal stabilities. Immobilized ionic liquid [HBth][PF_6] on ZIF-8 gave higher adsorptive performance over the other ionic liquid and ZIF-8 composites, which also showed the merits of better stability and easier preparation. The result proved that the adsorption properties of MOFs could be well improved by using appropriate ILs. Moreover, the adsorption conditions were optimized based on response surface methodology. The adsorption kinetics follow pseudo-second order model which revealed that the rate-limiting step is the interaction between the available surface sites and adsorbate. The enhanced adsorption achievement is mainly ascribed to the presence of IL within the adsorbent which gets involved in various interactions

including H-bonds, electrostatic interactions, anion-exchange and π-π combinations. Redlich-Peterson model is suitable to estimate the equilibrium adsorption amount, and the adsorption of target antibiotics onto IL@ZIF-8 was spontaneous which was endothermic in nature. The adsorbed TCs could be desorbed efficiently and the performance of the IL@MOF sorbent was further verified by actual water samples, which is expected to provide meaningful reference for related researchers.

CRediT authorship contribution statement

Alula Yohannes: Methodology, Experiments, Investigation, Writing - original draft.
Jing Li: Validation, Data analysis, Sample treatment.
Shun Yao: Conceptualization, Writing - review & editing, Supervision.

Declaration of competing interest

The authors declare that they have no known competing financial interests or personal relationships that could have appeared to influence the work reported in this paper.

Acknowledgements

Preparation of this paper was supported by 2017 “Stars of Chemical Engineering” outstanding young talent training program of Sichuan University. Special thanks to my wife and children for their support when I carried out researches in China.

References

[1] J. Jin, Z. Yang, W. Xiong, Y. Zhou, R. Xu, Y. Zhang, Sci. Total Environ. 650 (2019) 408–418.
[2] M. Khodadadi, M.H. Ehrampoush, M.T. Ghaneian, A. Allahresani, A.H. Mahvi, J. Mol. Liq. 255 (2018) 224–232.
[3] S. Shariati, Y. Yamini, A. Esrafili, J. Chromatogr. B 877 (2009) 393–400.
[4] H. Xu, H.Y. Mi, M.M. Guan, H.Y. Shan, Q. Fei, Y.F. Huan, Food Chem. 232 (2017) 198–202.
[5] Y.K. Lv, J.Q. Zhang, Y.D. He, J. Zhang, H.W. Sun, New J. Chem. 38 (2014) 802–808.
[6] H.D. de Faria, M.A. Rosa, A.T. Silveira, E.C. Figueiredo, Food Chem. 225 (2017) 98–106.
[7] S. Liu, M. Pan, Z. Feng, Y. Qin, Y. Wang, L. Tan, T. Sun, New J. Chem. 44 (2020) 1097–1106.
[8] X.Q. Yang, C.X. Yang, X.P. Yan, J. Chromatogr. A 1304 (2013) 28–33.
[9] M. Massoudinejad, M. Ghaderpoori, A. Shahsavani, M.M. Amini, J. Mol. Liq. 221 (2016) 279–286.
[10] H. Duo, H. Tang, J. Ma, X. Lu, L. Wang, X. Liang, New J. Chem. (43) (2019) 15351–15358.
[11] D. Wang, F. Jia, H. Wang, F. Chen, Y. Fang, W. Dong, J. Colloid Interface, Sci. 519 (2018) 273–284.
[12] L. Xia, L. Liu, X. Xu, F. Zhu, X. Wang, K. Zhang, X. Yang, J. You, New J. Chem. 41 (2017) 2241–2248.
[13] J. Panda, J.K. Sahoo, P.K. Panda, S.N. Sahu, R. Sahu, J. Mol. Liq. 278 (2019) 536–545.
[14] N. Lu, X. He, T. Wang, S. Liu, X. Hou, Microchem. J. 137 (2018) 449–455.
[15] L. Nie, J. Lu, W. Zhang, A. He, S. Yao, Sep. Purif. Technol. 155 (2015) 2–12.
[16] Y. Wang, L.S. Qian, Y.M. Miao, Y. Zhao, R.Y. Li, J.Y. Tang, Sep. Sci. Technol. 54 (2019) 3019–3026.
[17] Q.X. Luo, B.W. An, M. Ji, J. Zhang, Mater. Chem. Front. 2 (2018) 219–234.
[18] Y. Sun, H. Huang, H. Vardhan, B. Aguila, C. Zhong, J.A. Perman, A.M. Al-Enizi, A. Nafady, S. Ma, ACS Appl. Mater. Inter. 10 (2018) 27124–27130.
[19] C. Chen, Z. Wu, Y. Que, B. Li, Q. Guo, Z. Li, L. Wang, H. Wan, G. Guan, RSC Adv. 6 (2016) 54119–54128.
[20] C. Chen, N. Feng, Q. Guo, Z. Li, X. Li, J. Ding, L. Wang, H. Wan, G. Guan, J. Colloid Interface, Sci. 521 (2018) 91–101.
[21] N.A. Khan, Z. Hasan, S.H. Jhung, Chem. Euro. J. 20 (2014) 376–380.
[22] N.A. Khan, Z. Hasan, S.H. Jhung, Chem. Commun. 52 (2016) 2561–2564.
[23] X. Dai, T. Yao, D. Tang, H. Song, L. Peng, S. Yao, J. Mol. Liq. 219 (2016) 923–929.
[24] L. Wang, X. Wang, T. Zuo, Q. Sun, P. Liu, S. Yao, H. Song, J. Chem. Thermodyn. 72 (2014) 48–53.
[25] S.A. Dharaskar, K.L. Wasewar, M.N. Varma, D.Z. Shende, C.K. Yoo, Arab. J. Chem. 9 (2016) 578–587.
[26] N. Stock, S. Biswas, Chem. Rev. 112 (2012) 933–969.
[27] Priscilla Rocío-Bautista, Carla Martínez-Benito, Verónica Pino, Jorge Pasán, Juan H. Ayala, Catalina Ruiz-Pérez, Ana M. Afonso, Talanta 139 (2015) 13–20.
[28] Y.R. Lee, M.S. Jang, H.Y. Cho, H.J. Kwon, S. Kim, W.S. Ahn, Chem. Eng. J. 271 (2015) 276–280.
[29] Z. Hasan, J. Jeon, S.H. Jhung, J. Hazard. Mater. 209-210 (2012) 151–157.
[30] K. Fujie, H. Kitagawa, Coordin. Chem. Rev. 307 (2016) 382–390.
[31] M. Mohamedali, H. Ibrahim, A. Henni, Chem. Eng. J. 334 (2018) 817–828.
[32] F.P. Kinik, C. Altintas, V. Balci, B. Koyuturk, A. Uzun, S. Keskin, ACS Appl. Mater. Inter. 8 (2016) 30992–31005.
[33] L. Lv, Z. Jie, C. Huang, Z. Lei, B. Chen, Sep. Purif. Technol. 125 (2014) 247–255.